

## **AZIMUTHAL SQUARE ARRAY RESISTIVITY SOUNDING OF SHALLOW SUBSURFACE FRACTURE DISTRIBUTION IN PARTS OF THE EASTERN BASEMENT COMPLEX OF NIGERIA**

**George, A. M<sup>1</sup>, Okwueze, E. E<sup>1</sup> and Abong, A. A\*<sup>2</sup>**

*1* Department of Physics University of Calabar-Nigeria

*2* Department of Physics Cross River University of Technology, Calabar-Nigeria

---

**ABSTRACT:** *Azimuthal square array resistivity sounding method was carried out at twelve (12) locations within Parts of the Eastern Basement Complex of Nigeria. The field data were collected using ABEM Terrameter with other accessories. For square – array, the location of measurement point is the centre point of the square and array size of 28m and 42m, 56m and 70m were used and each square was rotated in 15<sup>0</sup> increments about the centre point for a total of 360<sup>0</sup>. Data were analyzed using Origin pro. 8.0 Software. The results of the study showed the presence of fracture zones and seven (7) of the fracture zones were oriented in the NE – SW direction, while six (6) were oriented in the NW – SE direction indicating that the study area is has good potentials for ground water development.*

**KEYWORD:** ABEM Terrameter, Basement, fracture, square array, resistivity, groundwater.

---

## **INTRODUCTION**

Portable water supply shortage in most of the crystalline bedrock environments of Southeastern Nigeria has become a source of worry to both the researchers and the inhabitants of the area. This shortage is as a result of increase in new settlements and agricultural activities in these communities. Borehole yield is generally low with yield factor of 0.1 to 0.4l/skm<sup>2</sup> (CRBDA, 2004). This is because the rocks within the study area are impermeable and impervious and groundwater depends exclusively on the discontinuities of the rocks (Okwueze et al., 1988). Due to this low yield, during dry season, water supplies from boreholes do not have long-term sustainability because adequate geophysical investigation has not been carried out to locate the productive zone in this area, so it is imperative to locate boreholes within the fractured and/or faulted basement rocks that seem to be prevalent in this area. Consequently, most boreholes drilled in these areas are either unproductive or sometimes have low yield. The presence of faults and/or fracture zones in a geologic medium contribute to the improvement of the hydrogeological characteristics such as the hydraulic conductivity and secondary porosity of such a medium, while also acting as a structural control for groundwater movement. Therefore quantifying these structures using geophysics would go a long way in assisting effective hydrogeological and engineering construction planning that may be required in similar environments in the future (Barker, 1992 and Barker et al, 1999).

Azimuthal resistivity method is an improvement of resistivity method where the magnitude and direction of the electrical anisotropy are determined. In this technique, an electrode is rotated about its centre so that apparent resistivity is observed for several directions (Taylor and Fleming, 1988).

### **Location and Geology of Study Area**

The study area is situated within the Oban Massif located between latitude  $5^{\circ}00'$  and  $5^{\circ}50'$  N and longitude  $8^{\circ}00'$  E and  $8^{\circ}50'$  E. Specifically, the study area lies between latitude  $5^{\circ}15'$  N and  $5^{\circ}27.5'$  N and longitude  $8^{\circ}15'$  E and  $8^{\circ}25'$  E (Figure 1). It covers an area of 198.125 sq.km. The study area lies within the tropical rain forest of Nigeria with two distinct seasons: wet season, which is between March and October and dry season which starts in November and ends in March. The mean temperature in the study area is about  $30^{\circ}\text{C}$  with a mean annual rainfall of 150 cm to 200 cm (CRBDA, 2004). Geologically, Oban Massif is a Precambrian basement complex located in Southeastern Nigeria surrounded by Cretaceous and young sedimentary rocks. Lithologically, three major rock groups are recognized in this region and are migmatitic and sheared gneissic rocks, older granite intrusive and unmetamorphosed dolerite to microdolerite intrusive (Figure. 2).

The Oban Massif is made up of two main sectors namely, the western sector (topographically subdued with higher human population density) and the eastern sector (topographically rugged country with peaks forested up to summits and sparse human settlements (Ekwere and Edet, 2012). The western sector is made up of gneisses, granites, quartzite, schist, dolerites, granodiorites and pegmatite, while the east is composed of migmatites, biotite-hornblende-gneisses, granites and amphibolites. The Oban Massif is underlain by highly deformed Precambrian crystalline rocks, mainly granites, gneisses and schist. These rocks exhibit varying degrees of weathering across the Massif. They are intruded by pegmatite, granodiorites, diorites, tonolites, monzonites, charnokites and dolerites (Ekwueme, 2003). The Oban Massif has a complex lithology and the differentiation of the rock types is difficult. One of the difficulties is due to the location of Oban Massif which is in the thick equatorial rainforest inhibited by wildlife. More so, rock outcrops in the area are generally intensely weathered thus making it difficult to see fresh rock for geological studies (Ekwueme et al, 1995). In terms of the rock ages, the oldest is the banded gneisses while diorite is the youngest rock in the Oban Massif.

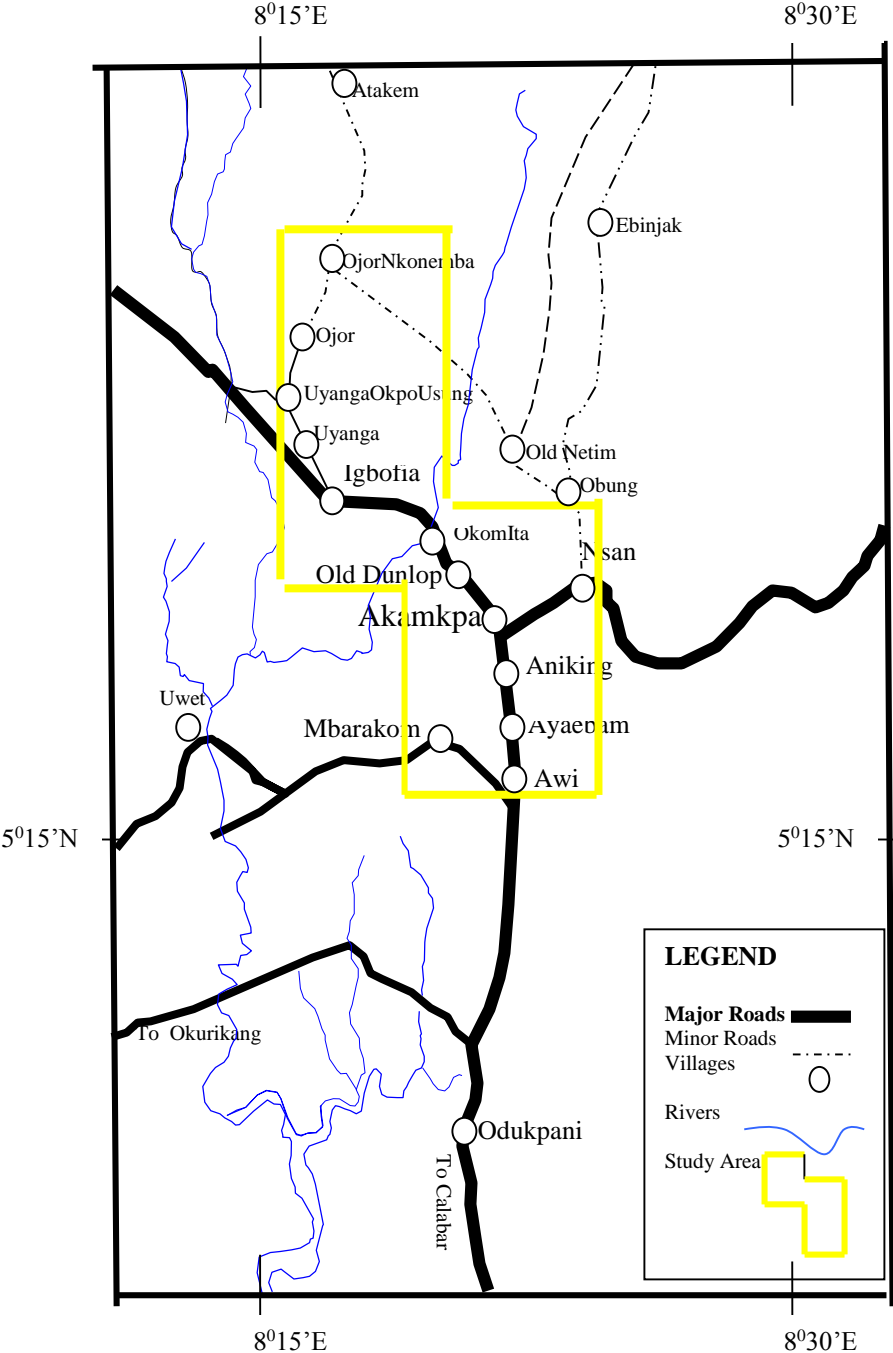


Figure 1 Location map of study area

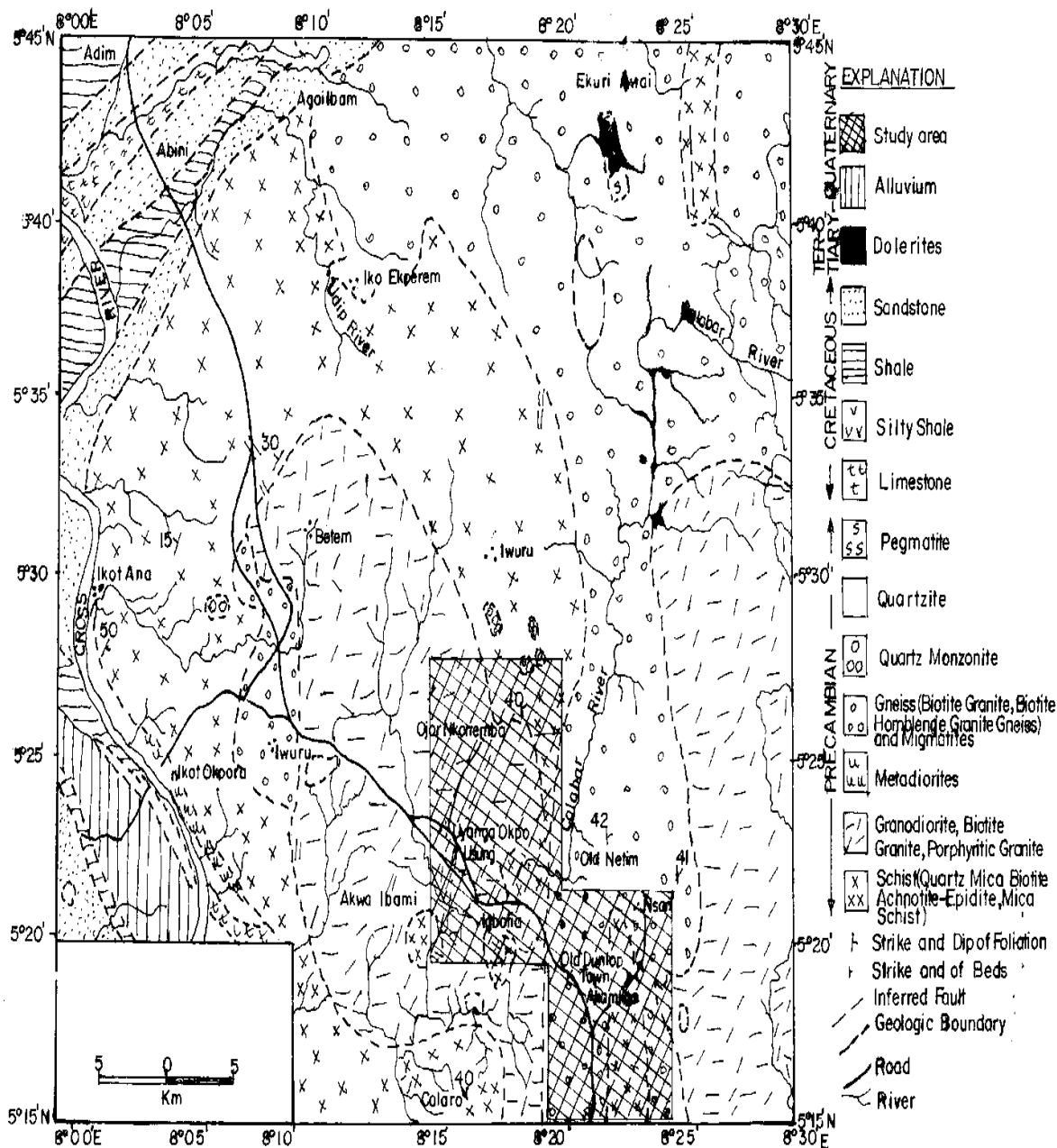


Figure 2: Geologic map of the study area

## LITERATURE/THEORETICAL BACKGROUND

Azimuthal resistivity technique has been used by many researchers to determine fracture geometry in crystalline rocks and glacial till (Ritzi and Andolsek, 1992; Lane et al, 1995 and Carlson et al, 1996), subsurface structures (Watson and Barker, 1999); fracture orientation (George et al, 2008); anisotropic studies (Ehirim and Essien, 2009); fracture in basement complex (Abdullah and Masanawa, 2012); investigate anisotropy and lateral effect (George and Abong, 2014).

The square array was originally developed as an alternative to Wenner or Schlumberger arrays when a dipping subsurface, bedding or foliation was present (Habberjam and Walkins, 1967). A dc-resistivity survey using the square – array method is conducted in a manner similar to that for traditional collinear arrays. The location of a measurement is assigned to the centre point of the square. The array size (A) is the length of the side of the square. The array is expanded symmetrically about the centre point, in increments of  $A\sqrt{2}$  so that the sounding can be interpreted as a function of depth.

For each square, three measurements are made, two perpendicular measurements (alpha,  $\alpha$  and Beta,  $\beta$ ) and one diagonal measurement (gamma,  $\gamma$ ) (Figure.3). The  $\alpha$  and  $\beta$  measurements provide information on the directional variation of the subsurface apparent resistivity ( $\rho_a$ ). The azimuthal orientation of the ( $\alpha$ ) and ( $\beta$ ) measurements is that of the line connecting the current electrodes. The measurement serves as a check on the accuracy of the measurements.

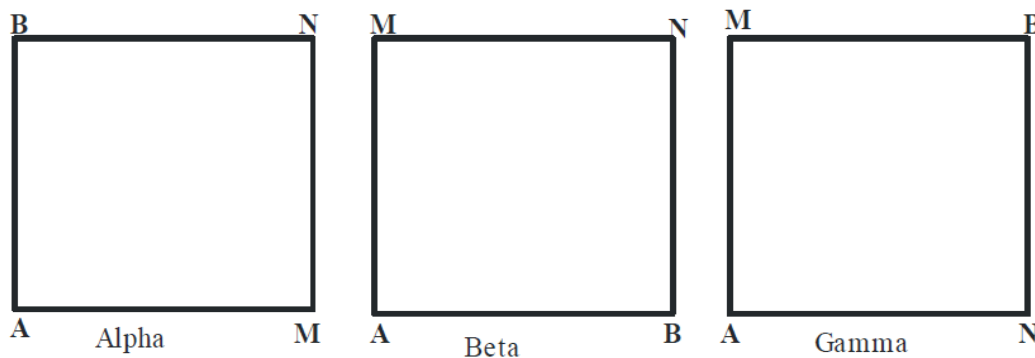


Figure.3 Electrode position for square-array measurement, AB represents current electrodes while MN represents potential electrodes.

In an Isotropic medium,

$$\rho_{\alpha\alpha} = \rho_{\beta\beta}, \text{ therefore } \rho_{\alpha\gamma} = 0$$

and in a homogeneous anisotropic medium

$$\rho_{\alpha\gamma} = \rho_{\alpha\alpha} - \rho_{\beta\beta}$$

where  $\rho_a$  = apparent resistivity in Ohm-meter.

For square – array configuration, the apparent resistivity is determined using the equation.

$$\rho_a = \frac{k\Delta V}{I}$$

where  $\rho_a$  = apparent resistivity, K = geometric factor for the array;  $\Delta V$  = potential difference in volts; and I = current magnitude, in amperes.

$$K = \frac{2\pi A}{2\sqrt{2}}$$

where A = square – array side length, in metres. In practice, multiple square-array data are collected at small angular intervals. In this study, square array data were collected with individual squares rotated at incremental angle of  $15^\circ$  to enable data to be presented on a rosette diagram for interpretation using Taylor and Fleming's (1988) Method.

## METHODOLOGY

The main field equipment used in this work was the ABEM Terrameter SAS 300 and theodolite. The ABEM Terrameter SAS 300 is a single unit consisting of a transmitter, a receiver, and a microprocessor. Others accessories of the SAS 300 used include the current cables, potential cables, stainless steel electrodes of length about 57cm, Nickel-Cadmium batteries, battery charger and Global positioning system (GPS).

For square – array, the location of measurement point is the centre point of the square and array size of 28.3m and 42.4m, 56.6m and 70.7m were used and each square was rotated in  $15^\circ$  increments about the centre point for a total of  $360^\circ$ . Field arrangement for azimuthal square array data collection is as shown in Figure4 and Figure 5. A total of 12 locations were sampled and the locations are denoted as AZS 01 to AZS 12.

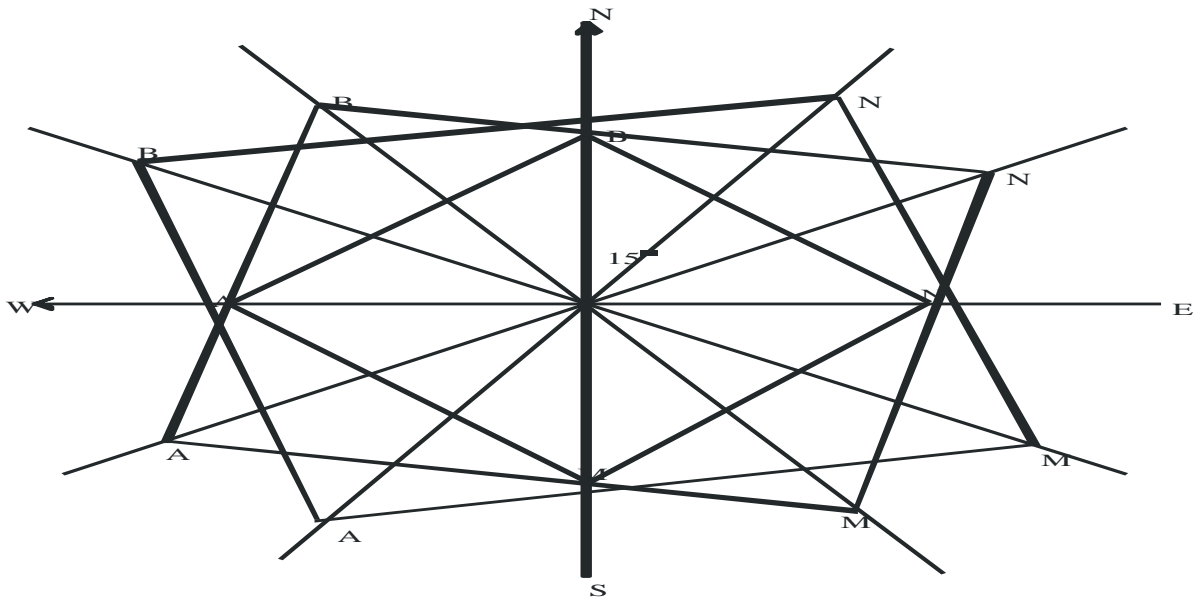
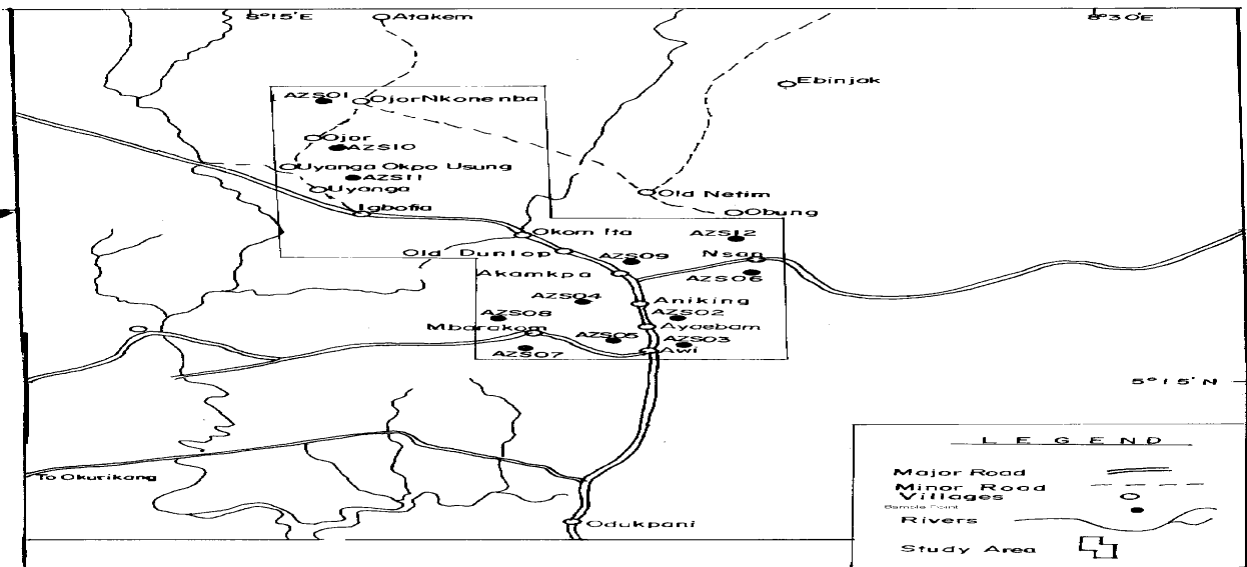


Figure 4: Field arrangement for azimuthal square array data collection,



AB = Current Electrodes, MN = Potential Electrodes

Figure 5: Layout of azimuthal square array survey at the study area

## Results/Findings

Data collected were analyzed by plotting the apparent resistivity against the azimuth for each “A” spacing using Originpro. 8.0 Software. Fracture strike can be determined graphically or analytically. In this work, the graphical analysis mode was used. In this mode, the value of apparent resistivity measurement for each square orientation is plotted against the azimuth for that square (Figure 5 – Figure 16). From the resulting azimuthal plot according to Habberjam (1975), the principal fracture strike direction for azimuthal square-array plot is perpendicular to the direction of maximum measured apparent resistivity.

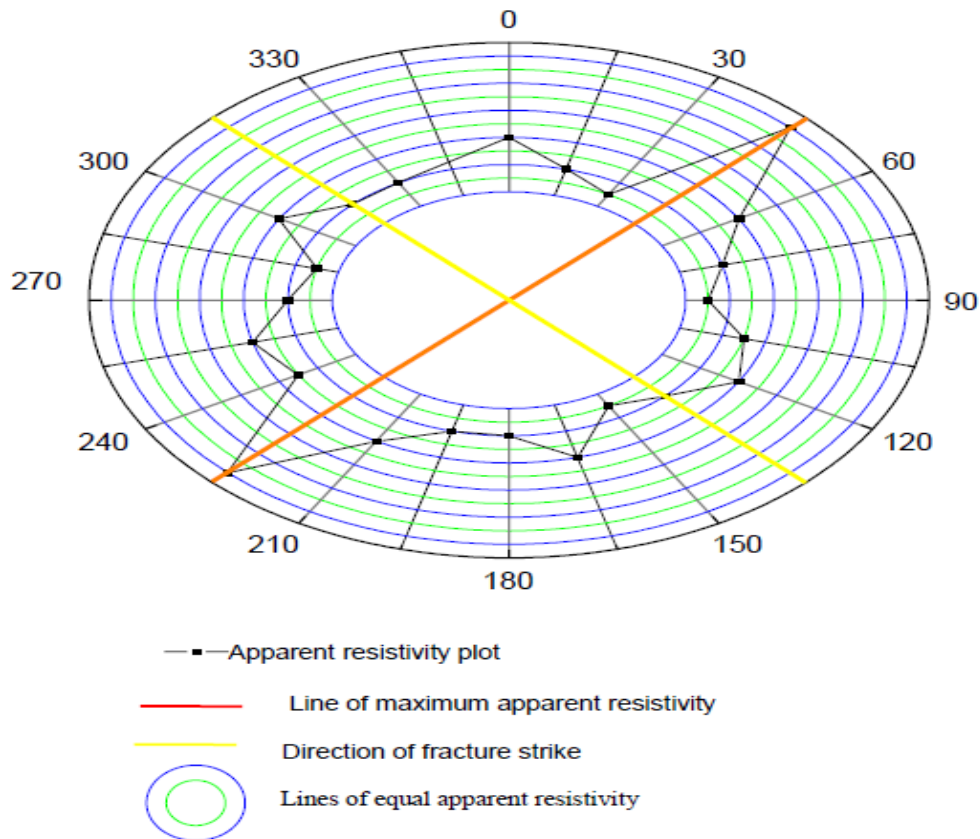


Figure 6: Apparent resistivity plot against azimuth with A=56m at location AZS01

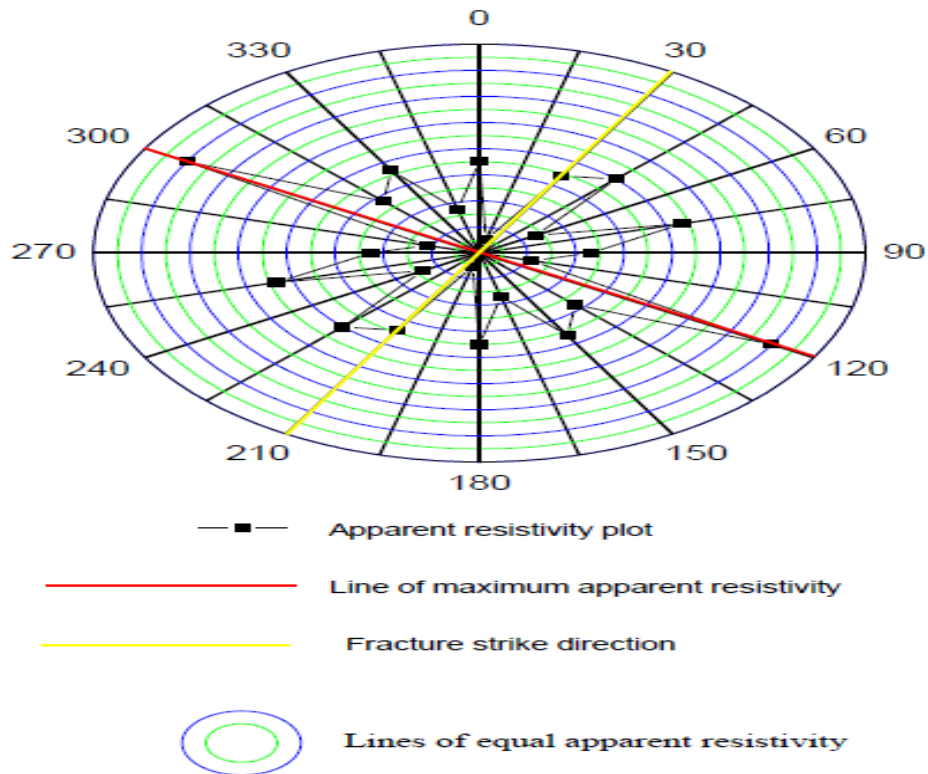


Figure 7: Apparent resistivity plot against azimuth with A= 42m and 56m at location AZS02

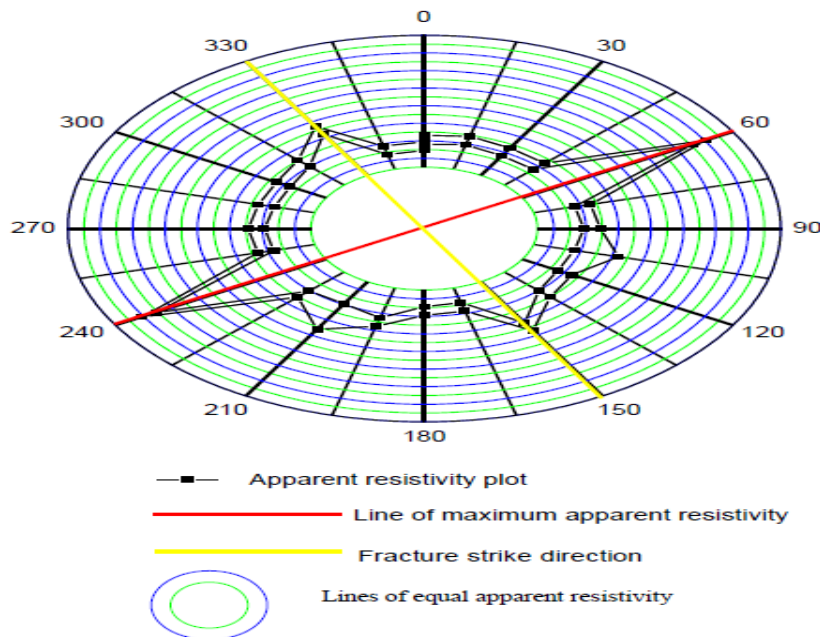


Figure 8: Apparent resistivity plot against azimuth with A=42m and A=56m at location AZS03

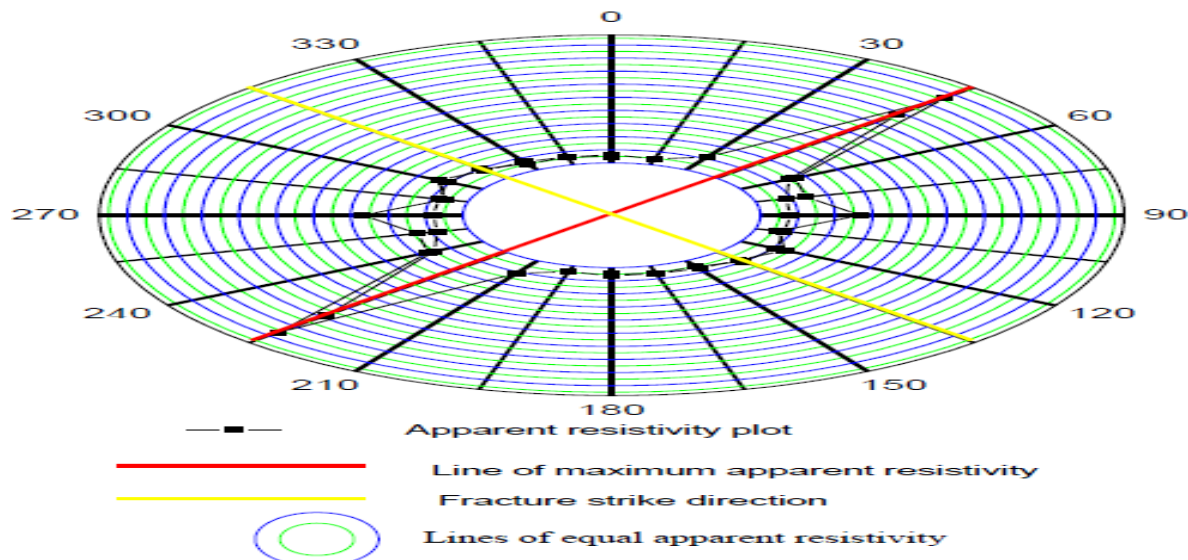


Figure.9 Apparent resistivity plot against azimuth with A=42m and A=56m at location AZS04

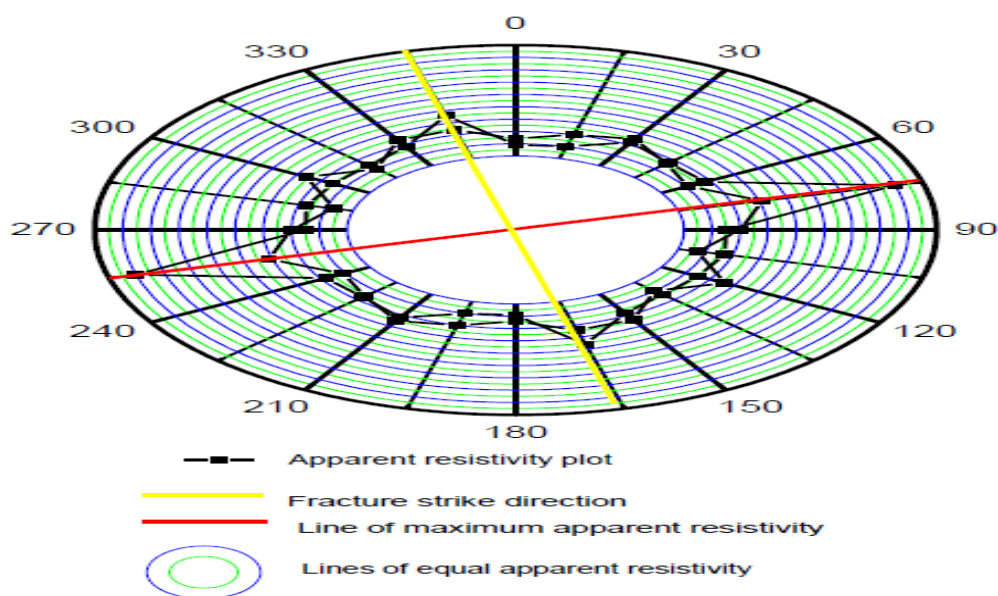


Figure.10 Apparent resistivity plot against azimuth with A=42m and A=56m at location AZS05

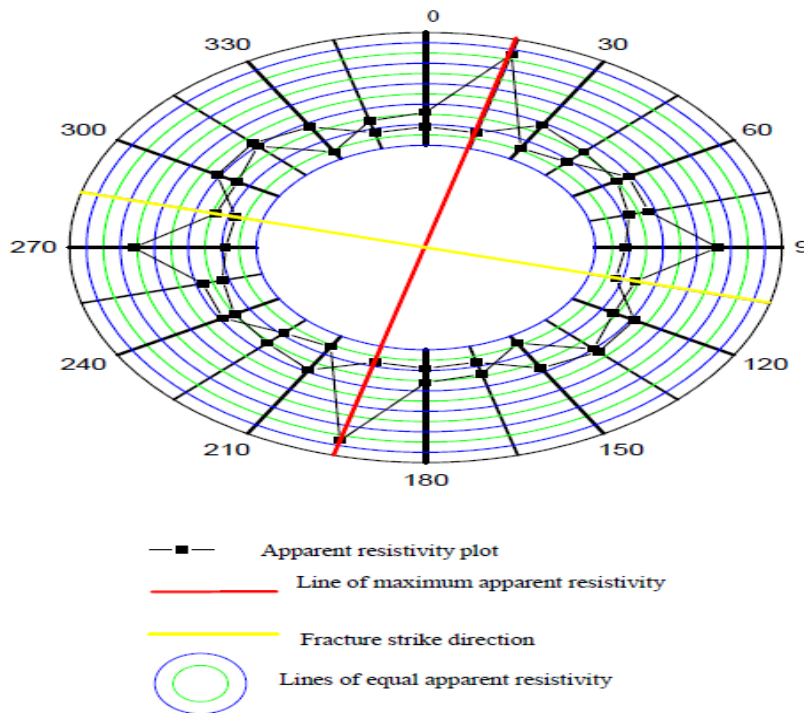


Figure 11: Apparent resistivity plot against azimuth with A=42m and A=56m at location AZS06

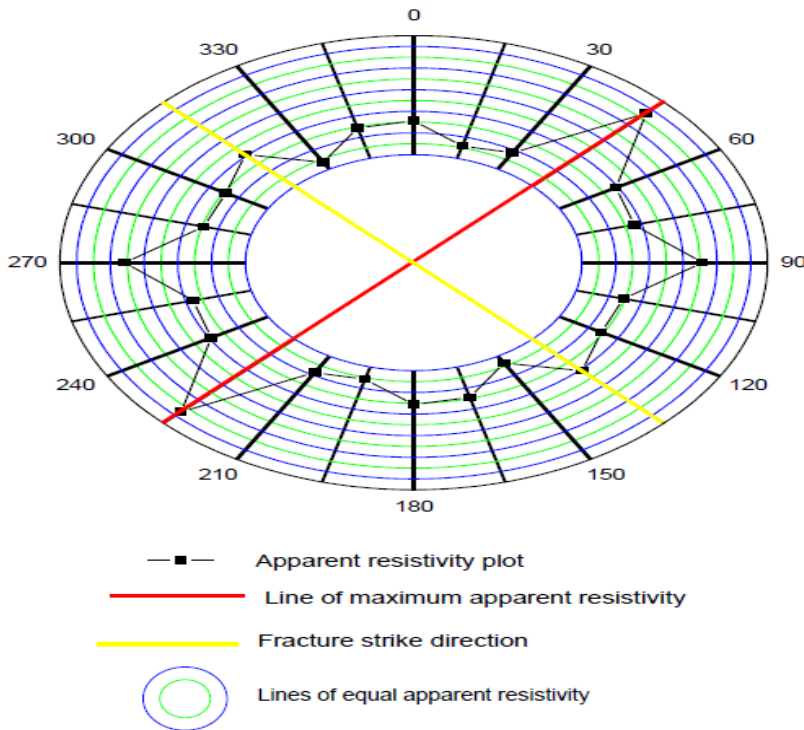


Figure 12: Apparent resistivity plot against azimuth with A=56m at location AZS07

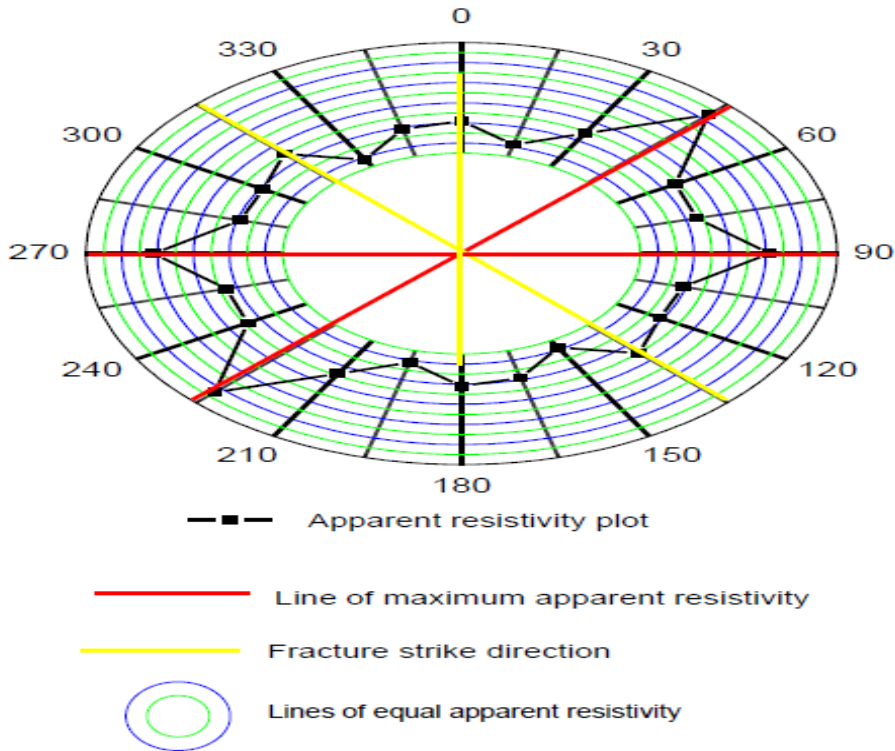


Figure 13: Apparent resistivity plot against azimuth with A=56m at location AZS08

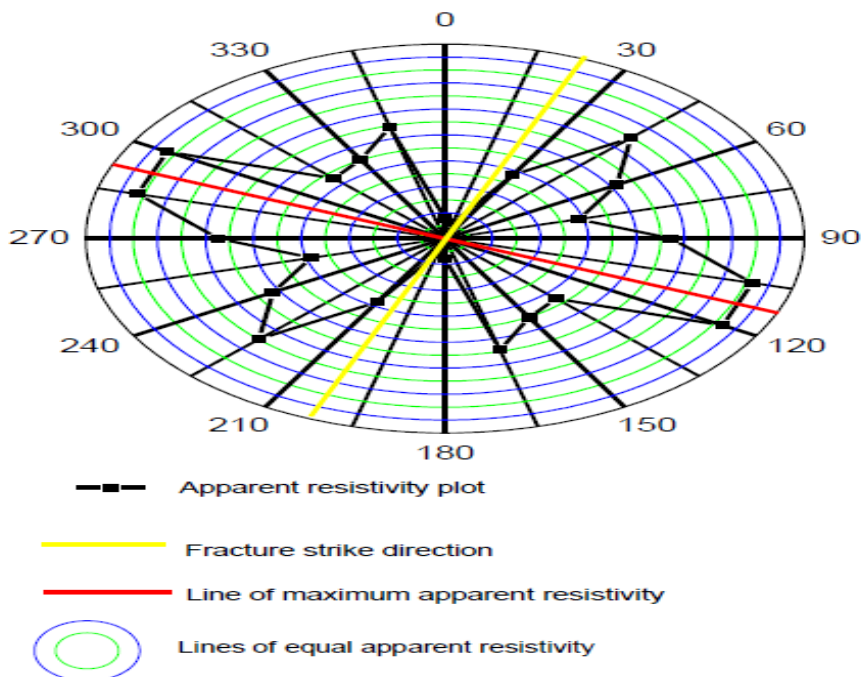


Figure 14: Apparent resistivity plot against azimuth with A=56m at location AZS09

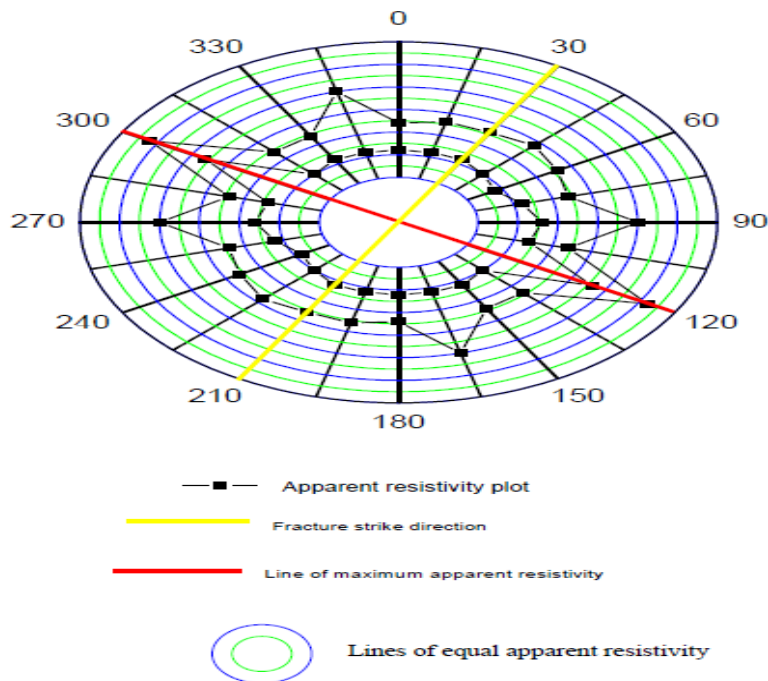


Figure 15: Apparent resistivity plot against azimuth with A=56m and A= 70m at location AZS10

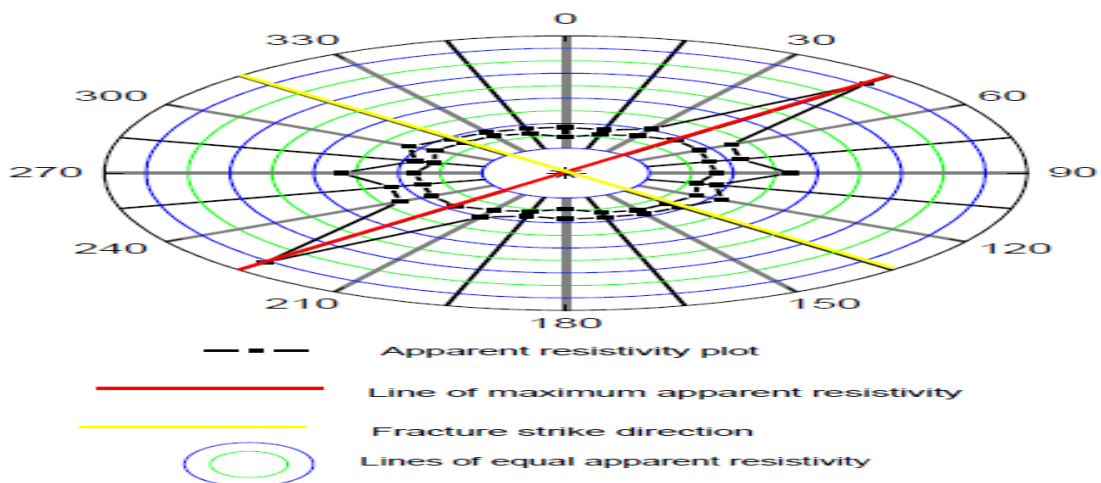


Figure 16: Apparent resistivity plot against azimuth with A= 28m and A= 56m at location AZS11

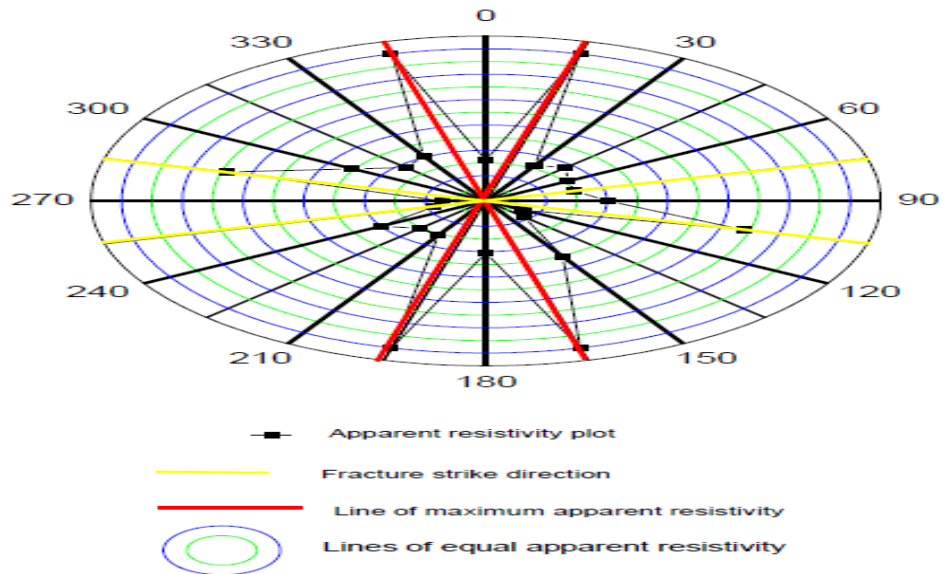


Figure 17: Apparent resistivity plot against azimuth with A=56m at location AZS12

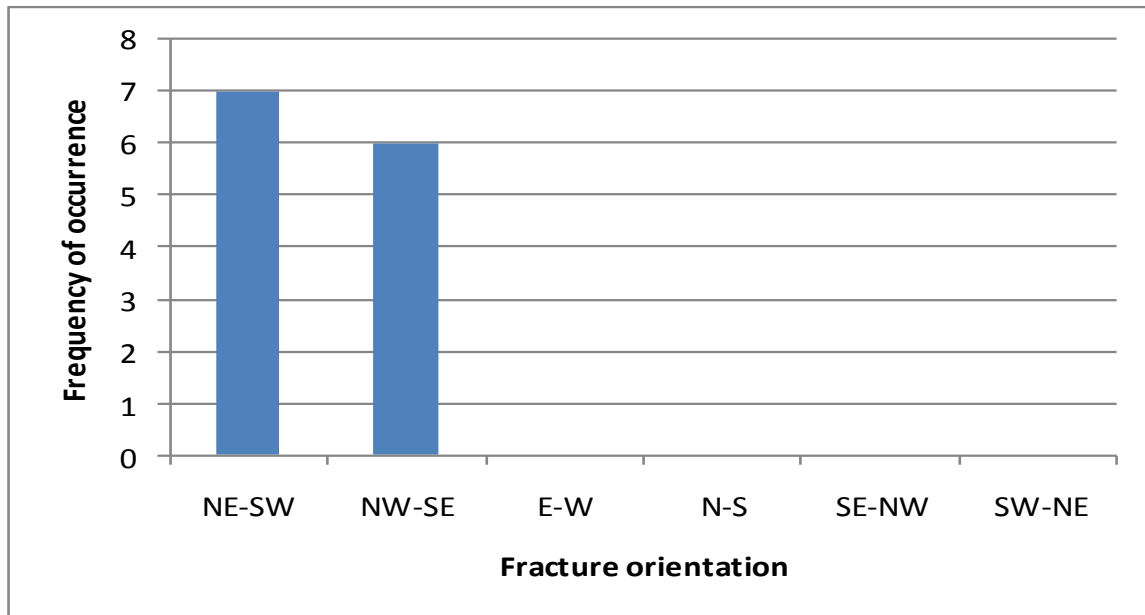


Figure 18: A plot of fracture frequency against fracture orientation

Table 1: Summary of results

<b>Location</b>	<b>A-spacing (m)</b>	<b>Fracture strike</b>
AZ 01	56.0	North (315 <sup>0</sup> ) East (NE-SW)
AZ 02	42.0, 56.0	North 210 <sup>0</sup> East (NE-SW)
AZ 03	42.0, 56.0	North 330 <sup>0</sup> East (NE-SW)
AZ 04	42.0, 56.0	North 315 <sup>0</sup> East (NW-SE)
AZ 05	42.0, 56.0	North 345 <sup>0</sup> East (NW-SE)
AZ 06	42.0, 56.0	North 285 <sup>0</sup> East (NW-SE)
AZ 07	56.0	North 315 <sup>0</sup> West (NW-SE)
AZ 08	56.0	North 315 <sup>0</sup> West (NW-SE) North-south
AZ 09	56.0	North 202.5 <sup>0</sup> West (NW-SE)
AZ 010	56.0, 70.0	North 030 <sup>0</sup> East (NE-SW)
AZ 011	28.0, 56.0	North 315 <sup>0</sup> West (NE-SW)
AZ 012	56.0	North 67.5 <sup>0</sup> East (NE-SW) North 105 <sup>0</sup> East (NE-SW)

## Discussion

The result of data collected at location AZS01 Figure.6 using “A”= 56m spacing, shows that the maximum apparent resistivity measured is parallel to  $045^{\circ}$ , resulting in a fracture strike oriented in North  $315^{\circ}$  East (NW – SE) direction. At location AZS02 Figure.7, a plot of measured apparent resistivity using “A”= 42m and 56m, shows maximum apparent resistivity parallel to  $120^{\circ}$ , resulting in fracture strike oriented in North  $210^{\circ}$  East (NE – SW) direction.

The plot of apparent resistivity against azimuth at location AZS03, Figure 8, using “A”= 42m and 56m spacing shows maximum measured apparent resistivity parallel to  $060^{\circ}$ . This results in fracture strike oriented in North  $330^{\circ}$  East (NE-SW) direction.

Similarly, at location AZS04 using “A”= 42m and 56m shows measured apparent resistivity parallel to  $045^{\circ}$  Figure.9. This gives rise to fracture strike oriented in North  $315^{\circ}$  East (NW – SE) direction. A plot of apparent resistivity against azimuth at location AZS05 Figure 10 shows the maximum measured apparent resistivity parallel to  $075^{\circ}$  for data collected using “A”= 42m and “A”= 56m. For this location the fracture strike is oriented in North  $345^{\circ}$  East (NW – SE) direction. At location AZS06, the maximum measured apparent resistivity is parallel to  $015^{\circ}$  Figure 11 for data collected using “A”= 42m and “A”= 56m. This results in fracture strike oriented in North  $285^{\circ}$  East (NW – SE) direction. Analysis of azimuthal square-array data collected at location ASZ07 shows maximum measured apparent resistivity parallel to  $045^{\circ}$  Figure 12, for “A”= 56m spacing. This results in fracture strike with orientation North  $315^{\circ}$  West (NW – SE) direction.

At location AZS08 Figure 13, two fracture zones were identified using “A”=56m spacing. The plot of apparent resistivity against azimuth at this location shows two directions for the maximum measured apparent resistivity. These apparent resistivity maximum were parallel to  $045^{\circ}$  and  $090^{\circ}$  respectively giving rise to fracture zones oriented North  $315^{\circ}$  West (NW – SE) and North – South direction respectively. Similarly, the result of azimuthal square-array data collected at location ASZ09 using “A”=56m spacing Figure 14 shows the maximum measured apparent resistivity parallel to  $112.5^{\circ}$ . This results in fracture zone with orientation North  $202.5^{\circ}$  West direction (NW – SE).

At location ASZ10 Figure 15, a plot of measured apparent resistivity against azimuth with “A”=56m and “A”=70m shows the maximum measured apparent resistivity parallel to  $300^{\circ}$  indicating that the fracture zone is oriented North  $030^{\circ}$  East (NE – SW) direction. At location ASZ11, a plot of apparent resistivity against azimuth using “A”=28m and “A”=56m Figure 16 shows the maximum measured apparent resistivity for “A”=56m spacing parallel to  $045^{\circ}$  indicating a fracture zone oriented North  $315^{\circ}$  West (NE – SW) direction. Two fracture zones were identified in location ASZ12 using “A”=56m spacing Figure 17. The maximum measured apparent resistivity as shown in the plot is parallel to  $015^{\circ}$  and  $345^{\circ}$  respectively. These result in fracture zones oriented North  $67.5^{\circ}$  East (NE – SW) and North  $105^{\circ}$  East (NE – SW) direction. A total of twelve (12) fracture zones with different orientations were identified using azimuthal square array electrodes configuration. Seven (7) of these were oriented in the NE – SW direction

while five (5) were oriented in the NW – SE direction. The frequency distribution of subsurface fracture orientation is as shown in Figure 18.

## CONCLUSION

The result of investigation shows the presence of subsurface fractures in the study area. The fracture zones with different orientations were identified using azimuthal square array electrodes configuration. Seven (7) of these were oriented in the NE – SW direction while six (6) were oriented in the NW – SE direction. The presence of fracture zones in all the sampled points in the study area shows that the study area has potentials for groundwater development as the presence and interconnectivity of fracture zones in the basement region serves as groundwater aquifer in the absence of reasonable overburden thickness.

## REFERENCES

- Abdullahi, N.K., Batu, M.A and Masanawa, A.A (2012) *Fracture determination using azimuthal, Schlumberger and offset Wenner array in Basement complex of Northern Nigeria*. Research Journal of Environment and Earth Sciences 4(7):747-755.
- Barker, R. D., White, C. C. and Houston, J. F. T. (1992) *Borehole siting in an African accelerated drought relief project*. In Wright, E. P. & Burgess, W. G. E (ed) Hydrogeology of Crystalline Basement Aquifers in Africa. London, Geological Society Special Publication 66, 183-201.
- Barker, R. D. (1999) *Surface and borehole geophysics*. In Lloyd, J. W (ed) Hardrock aquifers. Paris, UNESCO, 128-143.
- Carlson, D.A., Taylor, R.W. and Cherkauer, D.A. (1996) Azimuthal Electrical Resistivity as a tool for determination of the orientation of preferred hydraulic transmissivity for a Dolomite Aquifer in Southeastern Wisconsin. SAGEEP 1996 Meeting, Keystone, Colorado, USDA, *Expanded Abstracts*.
- Cross River Basin Development Authority (2004) *Groundwater Geologic map of Cross River State*. Survey and Mapping GEODATA Limited, Ikeja, Lagos.
- Ehirim, C.N and Essien, E.E (2009) *Comparative investigation of offset Wenner, square and Schlumberger arrays in electrical anisotropy studies*. Scientia Africa, 8(2):53-60.
- Ekwere, A.S, and Edet, A. (2012) *Trace metals in ground and surface waters of the Oban Massif area, SE Nigeria*. Advances in Applied Science Research, 3(1), 312-318.
- Ekwueme, B. N.; Nyong, E. E. and Peters, S. W. (1995) *Geological excursion guidebook to Oban Massif, Calabar flank and Mamfe Embayment, southeastern Nigeria*. Calabar, Dechord Press, 1-36.
- Ekwueme, B .N (2003) *The Precambrian geology and evolution of the Southeastern Nigerian basement complex*. University of Calabar Press, 2003, p135
- George, A. M., Okwueze, E.E., Akpan, A. E. and Uchegbu, C. J. (2008) *Comparative VES studies for the determination of fracture orientation using azimuthal square array and Schlumberger array data in Awi within the Oban Massif, S.E. Nigeria*. Nigerian Journal of Physics, 20(1), 136-144.

- George, A. M and Abong, A.A (2014) *DC Resistivity Investigation of anisotropy and lateral effect using azimuthal Offset Wenner Array. A case Study of the University of Calabar, Nigeria* Journal of Environment and Earth Science, 4(1), 53-60.
- Habberjam, G. M. and Watkins, G. E. (1967) *The use of square configuration in resistivity prospecting*. Geophysical Prospecting, 15, 221-235.
- Habberjam, G. M. (1975) *Apparent Resistivity, Anisotropy and strike measurements*. Geophysical Prospecting. 23, 211-247.
- Lane, J. W. jr.; Haeni, F. P. and Watson, W. M. (1995) Use of square array direct-current resistivity method to detect fractures in crystalline bedrock in New Hampshire. *Groundwater*, 33(3), 476-485.
- Okwueze, E. E., Umego, M. N., Baimba, A. A., Ntaji, F. A. and Ajakaiye, D. E. (1988) Application of geophysical methods to groundwater exploration in Nigeria. *Stygologia* 4(2): 103-115.
- Ritzi, R.W. and Andolsek, R.H. (1992) Relation between anisotropic transmissivity and azimuthal resistivity w, fractured, carbonate flow systems. *Ground Water*, 30(5): 774-780.
- Taylor, R. W. and Fleming, A. H. (1988) Characterizing jointed systems by azimuthal resistivity surveys. *Groundwater*. 26(4), 464-474.
- Watson, K.A. and Barker, R.D. (1999) Differentiating anisotropy and lateral effects using azimuthal resistivity offset Wenner soundings. *Geophysics*, 64(3): 739-745.